J. Fluid Mech. (1988), *vol.* 194, *pp.* 175–186
Printed in Great Britain

A note on lateral heating in a double-diffusive system

By T. L. BERGMAN† AND A. UNGAN‡

† Department of Mechanical Engineering, The University of Texas at Austin, Austin, TX 78712, USA

‡ School of Engineering and Technology at Indianapolis, Division of Engineering, Purdue University, Indianapolis, IN 46260, USA

(Received 9 July 1987 and in revised form 10 January 1988)

An experimental investigation of double-diffusive convection in a two-layer, salt-stratified solution destabilized by lateral heating and cooling has been performed. Initially, diffusive regime phenomena are observed as the two uniform salinity layers are thermally driven and behave somewhat independently. As salt is transferred across the interface separating the layers, salinity stabilization decreases and complicated flow structure is observed at the interface. In the final stages before mixing, the stabilizing salinity gradient becomes small, the thermal/hydrodynamic boundary layers on the heated and cooled sidewalls penetrate the salinity interface and mixing, in the finger regime, occurs. The dimensionless mixing time is described with parameters associated with thermal and salinity buoyancy forces and the enclosure aspect ratio. Careful selection of the experimental conditions allows dimensionless interfacial salinity transport rates to be correlated with appropriate dimensionless parameters.

1. Introduction

Double-diffusive natural convection occurs in fluids when two components contribute to its density and diffuse at different rates. Natural convection systems that involve the simultaneous interaction of two components, such as heat and a solute, are considerably more complex than those associated with the driving force from only one diffusing component and a range of unexpected fluid motion can occur (Turner 1979).

Although most investigations of double-diffusive phenomena have considered the diffusive or finger regimes (Turner 1979), it has been noted that convective systems driven by sidewall heating or cooling can also display double-diffusive characteristics (Ostrach 1980). These investigations have, for the most part, considered linearly solute-stratified fluids which are heated or cooled from vertical walls (for example, Huppert, Kerr & Hallworth 1984), and the subsequent formation, interaction and merging of vertically-stacked, horizontal convective layers. More recently, experiments have been performed to elucidate fluid motion relevant in various crystal growth schemes in which a fluid with an initially uniform concentration was contained in an enclosure with heated and cooled sidewalls held at two different concentrations (Kamotani *et al.* 1985). Unusual convective patterns were noted and consisted, as in the previous case, of discrete horizontal, uniform concentration layers. The layers were present regardless of whether the temperature and concentration distributions produced augmenting or counteracting density varia-

tions and their presence was attributed to double-diffusive phenomena. The layering phenomena encountered in these systems is similar to that of an early investigation involving discrete layers of solute-stratified fluid heated or cooled at the vertical walls of an enclosure (Wirtz & Reddy 1976; Wirtz 1977; Wirtz & Reddy 1979). In these studies, double-diffusive interactions were noted at the interface separating the two fluid layers, which is the location of stable and unstable vertical solute and temperature gradients, respectively.

Although layered structures exist in all of the work described above, little consideration has been given to a detailed investigation of the interaction of individual layers, the heat and species transport through the interface separating the layers, and layer merging at marginal interface stabilities. The purpose of this study is to consider the transient behaviour of a solute-stabilized, discretely layered system destabilized by lateral heating and cooling. Unlike the previous investigations, consideration will be given to all phases of system behaviour; from the initiation of thermally-driven convection, through quasi-steady behaviour, to layer breakdown and merging. Species transport rates across the interface, which ultimately govern the stability and merging of fluid layers, will be correlated with appropriate dimensionless parameters.

2. Experiments

The physical system under consideration is shown in figure 1. Initially, two fluid layers of equal depth, but different solute concentrations (C_1 and C_2), are contained within an enclosure. The enclosure walls are impermeable and are adiabatic at the bottom ($y = 0$) and the top ($y = H$) while the sides are maintained at temperatures T_1 on the left wall ($x = 0$) and T_2 on the right wall ($x = L$). For all of the experiments, $T_1 > T_2$. With this arrangement, thermal buoyancy forces induce clockwise motion in the system while solutal buoyancy forces tend to inhibit layer mixing. The interface separating the two layers is characterized by shear instabilities due to the clockwise rotation of each fluid layer, as well as double-diffusive instabilities since the solutal and thermal buoyancy forces are stabilizing and destabilizing at this location, respectively. The resulting heat and solute transport through the interface will influence the lateral heat transfer rates across the enclosure as well as the lifetime of the layered structure. A steady state will eventually occur when the concentrations of the two layers become equal and the system corresponds to the well-studied case of a simple fluid in an enclosure with differentially heated sidewalls.

2.1. *Governing dimensionless parameters*

Before describing the experiments in detail, it is useful to consider the dimensionless parameters which govern the system's behaviour.

Although the system behaviour is transient, a quasi-steady period exists between the onset of thermal convection and layer merging (Wirtz 1977). During this time, the thermally-induced convection is only slightly affected by solute transfer. The fluid motion is characterized by two large rotating cells above and below $y = \frac{1}{2}H$ and is governed by the following dimensionless parameters which may be obtained through formal normalization of the continuity, momentum, energy and species equations:

Prandtl number, the ratio of momentum to thermal diffusivities,

$$Pr = \nu/\alpha; \tag{1}$$

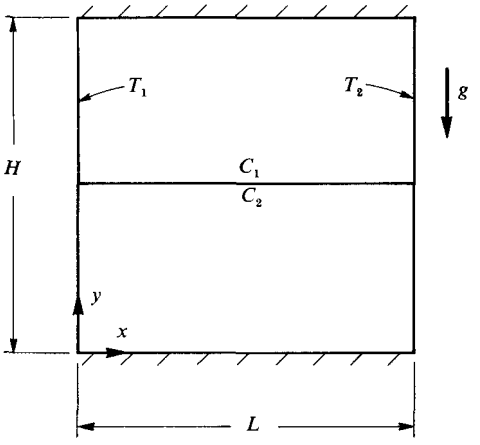

FIGURE 1. Schematic of the physical system.

thermal Rayleigh number, the ratio of thermal buoyancy to viscous forces,

$$Ra_T = \frac{g\beta_T(T_1 - T_2)}{\nu\alpha} L^3; \tag{2}$$

Schmidt number, the ratio of momentum to species diffusivities,

$$Sc = \nu/D; \tag{3}$$

buoyancy ratio, the ratio of solutal to thermal buoyancy forces,

$$R_\rho = \beta_C(C_2 - C_1)/\beta_T(T_1 - T_2); \tag{4}$$

and the test-cell aspect ratio,

$$A = H/L. \tag{5}$$

The fluid properties in (1)–(5) are the kinematic viscosity, ν, thermal diffusivity, α, and the binary diffusion coefficient, D. The density of the fluid is written with a linear approximation

$$\rho = \rho_0[1 - \beta_T(T - T_0) + \beta_C(C - C_0)], \tag{6}$$

and ρ_0, T_0 and C_0 are reference quantities. The linear expansion coefficients, β_T and β_C, are defined as

$$\beta_T = -\frac{1}{\rho}\left|\frac{\partial\rho}{\partial T}\right|_C; \quad \beta_C = \frac{1}{\rho}\left|\frac{\partial\rho}{\partial C}\right|_T. \tag{7}$$

Here, the gravitational acceleration is represented by the symbol g. It should be noted that the difference in the layer solute concentrations, $C_2 - C_1$, and hence R_ρ, will decrease with time in a particular experiment due to species transport across the interface.

The parameters in (1)–(5) are the same as those which govern pure fluids except for Sc and R_ρ. The Schmidt number and buoyancy ratio are important because they influence the shape and structure of the interface separating the two fluid layers. For example, large R_ρ correspond to stable interfaces while small R_ρ are associated with less stable interfaces. The thickness of the interface is influenced by the extent of the concentration boundary layers on either side of it and, hence, on the relative rates of momentum and solute diffusion (Sc).

The dimensionless temporal response of the system can be described by the thermal and solutal Fourier numbers,

$$Fo_T = \frac{\alpha t}{L^2}; \quad Fo_C = \frac{Dt}{L^2}, \tag{8}$$

where t is time. The ratio of the thermal and solutal Fourier numbers yields the Lewis number, which is also the ratio of thermal and species diffusivities,

$$Le = \alpha/D. \tag{9}$$

Since Le is large (order 100) for binary liquids, the system's thermal response is much faster than its solutal response and the quasi-steady portion of the experiment may be thought of as the intermediate period between the thermal and solutal response.

As $C_2 - C_1$ approaches zero, layer mixing will occur. Mixing (merging) is associated with a solutal mixing Fourier number,

$$Fo_{C,\mathrm{m}} = \frac{Dt_{\mathrm{m}}}{L^2}, \tag{10}$$

where t_{m} is the time associated with mixing.

2.2. *Experimental techniques*

Experiments were performed using a rectangular test cell whose top, base, front and back were made of acrylic while the sidewalls were multipass copper heat exchangers (figure 2). One of the heat exchangers was wedged between the front and back test-cell walls and could be moved to vary L. Likewise, the acrylic test-cell top was wedged between the heat exchangers, allowing variation of H. The third dimension of the test cell was 200 mm and its walls, bottom and top were insulated with 25 mm styrofoam sheets which could be removed to perform flow visualization. Details of the test cell and its construction are provided elsewhere (Stickles, Ungan & Viskanta 1986).

The test cell was filled with two layers of uniform salinity (NaCl) water by carefully introducing a fresh water layer above a salty layer with a floating sponge arrangement. The salinity of the bottom layer was accurately established to within an estimated 5% by mixing a known volume of 10 wt% salt water with a known amount of fresh water. The interface at $y = \frac{1}{2}H$ was observed to be very sharp (thickness of order 1 mm) at the onset of convection in each experiment.

The heat exchanger fluid was provided by two constant temperature circulators. The circulating fluid temperature was allowed to reach T_1 and T_2 and was measured to within 0.01 °C with a quartz thermometer prior to the start of each experiment. The copper heat exchanger temperatures varied from their set points upon initiation of the experiment due to their thermal mass, but reached T_1 and T_2 within several minutes.

Flow visualization and qualitative temperature measurements were performed with neutrally-buoyant, polystyrene-encapsulated liquid crystals which were illuminated by a 5 mm wide vertical sheet of white light (Rhee, Koseff & Street 1984). This temperature measurement technique was chosen in lieu of conventional techniques, such as thermocouples, since preliminary experiments showed that the flow patterns and temperature distributions are very complex and specific locations of interest, such as at the interface, migrate during the course of the experiment. Hence, temperature data obtained at a particular location do not provide much insight into the system's behaviour. An additional complexity was discovered during

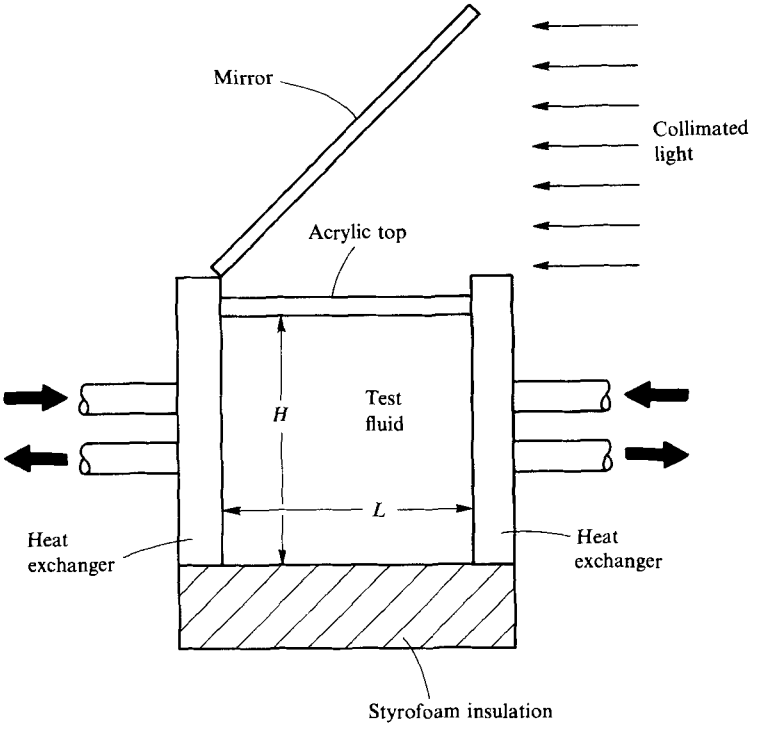

FIGURE 2. Schematic of the test cell and experimental apparatus.

the preliminary experiments when it was found that a relatively small initial concentration difference was necessary to promote layer merging in a reasonable time (hours rather than days). Unfortunately, the small concentration differences used in the experiments preclude accurate salinity measurement during the course of an experiment. That is, the uncertainty in refractometric measurements (with an Abbe refractometer) or polarigraphic measurements (Wirtz & Reddy 1979) is of the same order of magnitude as the initial concentration difference. Conventional optical flow visualization tools, such as the shadowgraph, were also ineffective due to the small concentration differences and test-cell size. As will become evident, these unavoidable difficulties do not limit the ability to describe system behaviour.

The experiments were performed in a temperature and humidity-controlled environmental chamber. This precaution was necessary for two reasons. First, the initial temperature, T_i, was established midway between T_1 and T_2. Since the liquid crystals were characterized by a colour range corresponding to a temperature range of 20 °C to 25 °C, T_i had to be consistently maintained at 22.5 °C, necessitating control of ambient conditions. (Although T_i was always 22.5 °C, $\Delta T = T_1 - T_2$ was varied from 5° to 15°.) Secondly, humidity control was necessary since, at normal ambient humidities, the fresh water would cool below 22.5 °C during test-cell filling because of evaporative heat losses, resulting in undesirable thermal convection which would destroy the marginally stable interface prior to the start of the experiment. To minimize these problems, the entire experiment was placed in the environmental chamber which was maintained continuously at 22.5 °C and a high ($\approx 100\%$) relative humidity.

The mixing time, t_m, was determined by visually observing the core of the fluid

Experiment	L (mm)	A	ΔT (°C)	ΔC (wt%)	$Ra_T \times 10^{-6}$	$R_{\rho,i}$	t_m (min)	$Fo_{c,m} \times 10^3$
A	50	1	5	0.1	8.65	0.59	44	1.89
B	50	1	10	0.2	17.00	0.59	38	1.63
C	50	1	15	0.3	25.50	0.59	34	1.46
D	100	1	5	0.1	69.00	0.59	111	1.19
E	100	1	10	0.2	138.00	0.59	70	0.75
F	100	1	15	0.3	207.00	0.59	35	0.38
G	50	2	5	0.1	8.65	0.59	53	2.28
H	50	2	10	0.2	17.00	0.59	45	1.94
I	50	2	15	0.3	25.50	0.59	41	1.76
J	50	1	5	0.2	8.65	1.17	195	8.38
K	100	1	15	0.6	25.50	1.17	143	6.14
L	50	1	5	0.2	69.00	1.17	370	4.00
M	100	1	15	0.6	207.00	1.17	240	2.57

TABLE 1. Experimental conditions and results

layer and was denoted as the time when relative motion of the tracer particles could no longer be distinguished. The uncertainty in t_m during a given experiment is estimated to be ± 60 s.

3. Results

Thirteen experiments were performed with various Ra_T, A and the initial buoyancy ratio, $R_{\rho,i}$. The Prandtl and Schmidt numbers for the experiments were approximately 6.5 and 550, respectively.

The conditions and results associated with each experiment are listed in table 1. Experiments A–I correspond to $R_{\rho,i} = 0.59$ while experiments J–M are characterized by $R_{\rho,i} = 1.17$. It should be noted that several of the experiments were performed more than once to ascertain the repeatability of observed system behaviour and t_m. In general, t_m was repeatable to within 10% from one experiment to the next and the discrepancy is attributed to perturbations introduced when filling the test cell.

3.1. *Flow visualization of system hydrodynamics*

Figure 3 (plates 1 and 2) shows representative flow visualization results obtained during experiment D. The time exposure of each photograph is 8 s. Streaklines are readily apparent while warm temperatures are associated with blue shades and cool temperatures correspond to red hues. The left wall is held at the warmer temperature.

Prior to the start of the experiment, no convective motion was evident. After initiation of sidewall heating, two large convective cells, above and below the interface, formed and are shown in figure 3(*a*) ($t = 10$ min). As evident, the salinity interface is not horizontal, rather, it is slightly tilted due to the lateral temperature gradient. The interface is the location of significant upward heat transfer and thermally-unstable density distributions, resulting from cool fluid travelling from the cold wall to the warm wall above the interface and warm fluid flowing in the opposite direction below the interface. Presumably, substantial stabilizing salinity gradients also exist at this location, rendering the interface overall stable. Superimposed on the bulk flow are hydrodynamic disturbances (waves) with a characteristic length of approximately 10 mm, as well as a thin core trapped between the two interfacial boundary layers. The hydrodynamic characteristics of the

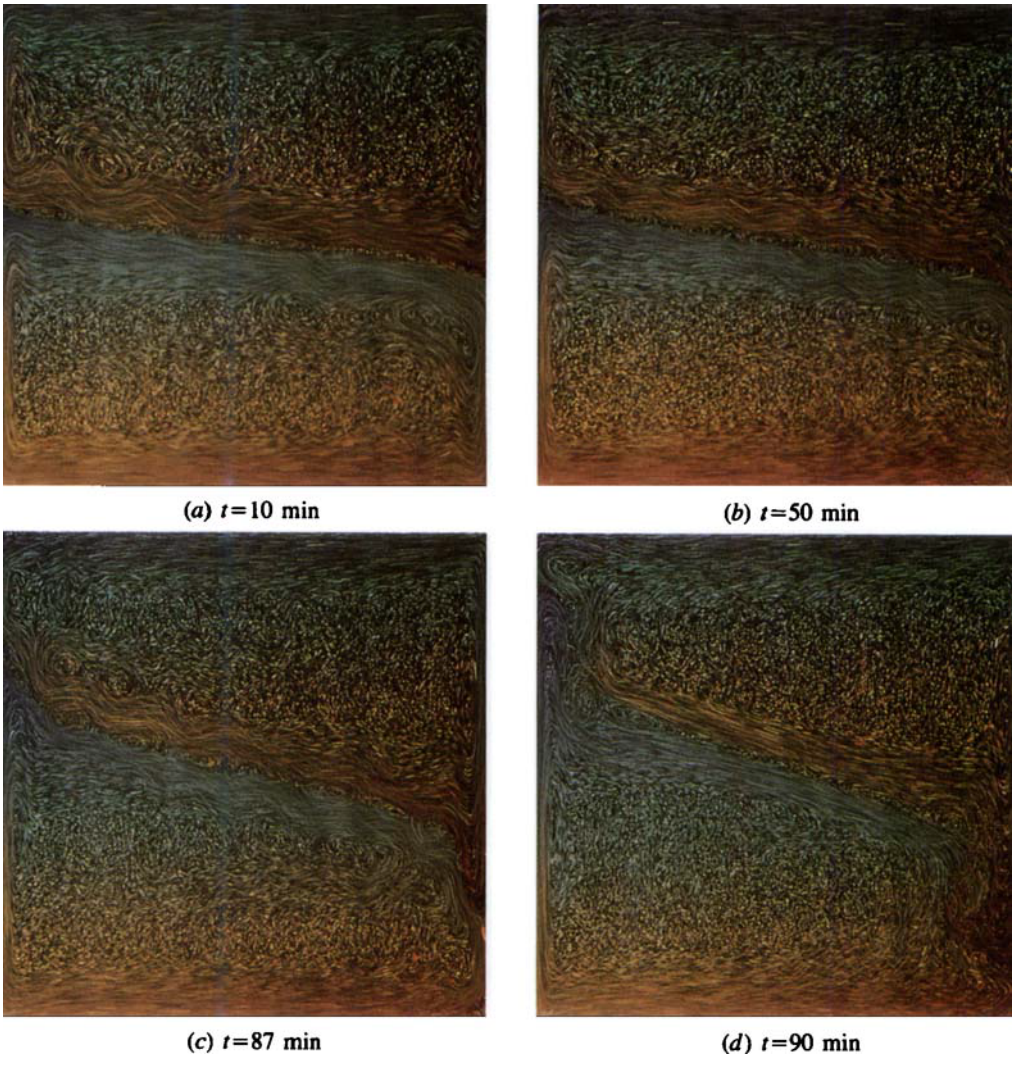

(*a*) $t=10$ min (*b*) $t=50$ min

(*c*) $t=87$ min (*d*) $t=90$ min

FIGURE 3. (*a*) – (*d*). See overleaf for caption.

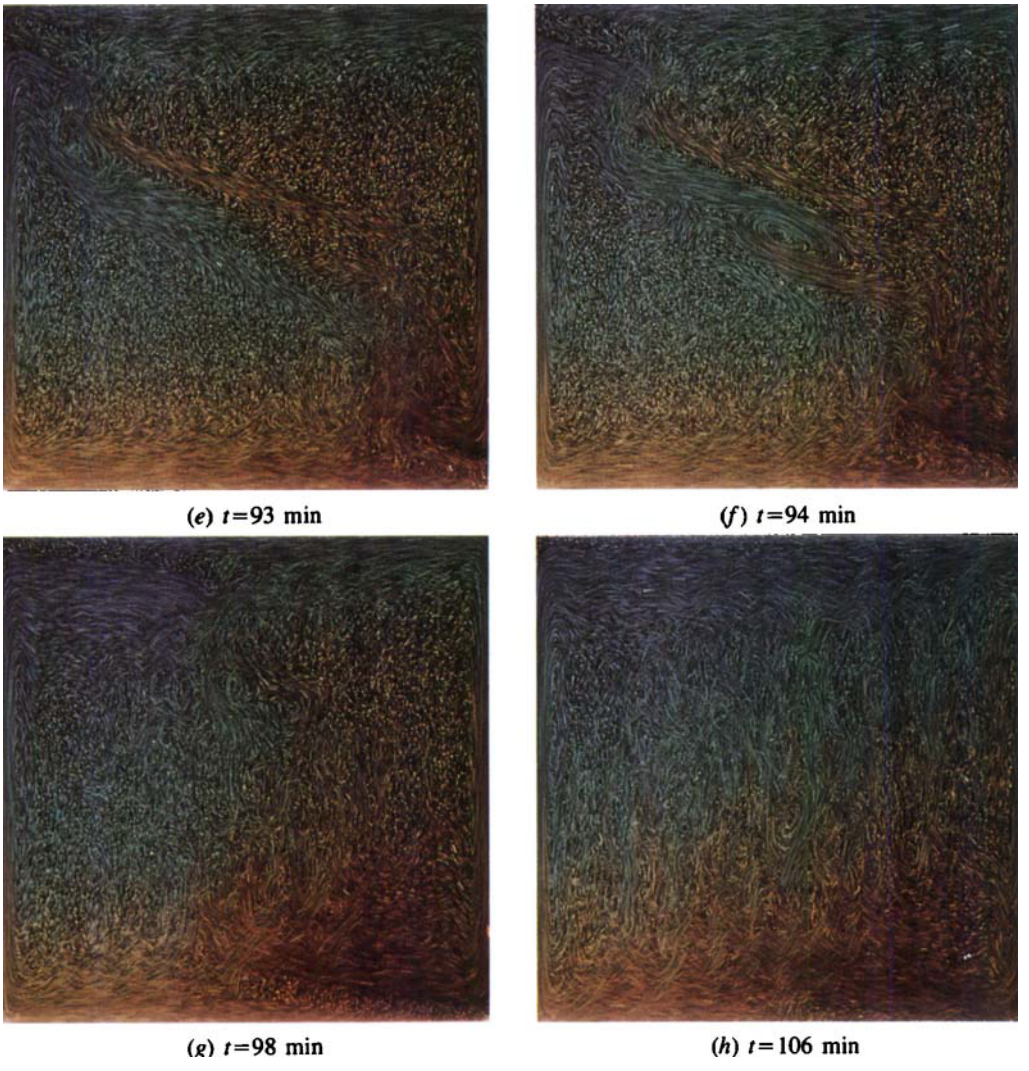

(*e*) $t=93$ min (*f*) $t=94$ min

(*g*) $t=98$ min (*h*) $t=106$ min

FIGURE 3. Flow visualization of experiment D.

interface may be induced by shear instabilities (Moore & Long 1971) however, double-diffusive effects can also influence the secondary structure (Linden & Shirtcliffe 1978). Secondary circulation is also evident on the upper left and lower right of the interface.

Since the thermal response time is less than its salinity counterpart, it is expected that quasi-steady behaviour will exist during a significant portion of the experiment. Figure 3(*b*) reveals the flow structure at $t = 50$ min. The characteristics of the flow at 50 min are strikingly similar to that observed in figure 3(*a*) and substantiates the notion of a relatively long quasi-steady state. As will be seen, the existence of the quasi-steady portion of the experiment will allow correlation of species transfer rates through the interface.

As previously mentioned, salt transport continuously occurs from the salty bottom layer to the relatively fresh top layer. As such, R_ρ decreases during the course of an experiment. The quasi-steady behaviour continues until R_ρ decreases to the point where the vertical boundary layers on the heated and cooled sidewalls begin to penetrate the salinity interface. Penetration is shown in figure 3(*c*) at $t = 87$ min. At this time, the interface is more tilted, relative to that of earlier times, and secondary flow at the interface becomes very evident where tiny vortices are trapped between the boundary layers.

Due to the penetration of the interface by the vertical boundary layers, it may be expected that enhanced salt transport between the layers begins to occur due to mixing near the test-cell walls (Wirtz & Reddy 1979). This hypothesized, enhanced mixing may be responsible for the ensuing rapid changes in the system dynamics.

Figure 3(*d*) corresponds to an experimental time of 90 min. Here, warm and cool sidewall boundary layers occupy almost all of the left and right sidewalls of the enclosure, respectively. Surprisingly, the secondary structure at the interface has disappeared.

Because of the tilting interface, the salty water below the interface becomes, in an integral sense, warmer than the relatively fresh layer above the interface. The effect of the biased heating of the layers can easily be seen in figure 3(*e*) ($t = 93$ min) with most of the salty water being warm (blue) and most of the fresh water being cool (red). Also of note is the relative decrease of fluid velocities at the geometrical centre of the system. In fact, this stagnation precedes local flow reversal and the formation of a small, clockwise vortex shown in figure 3(*f*) ($t = 94$ min).

The central vortex was observed each of the four times experiment D was performed and was characterized by surprisingly large rotational speeds (it was relatively difficult to visually observe the interfacial flow of figures 3(*a*)–3(*d*), but the vortex of 3(*f*) was always easily seen with the naked eye). The lifetime of the vortex is short, typically less than 30 s, but it consistently provided a clear signal that complete mixing is imminent.

Due to the preferential heating of the higher salinity fluid, and the continuing rotation of the interface, warm, salty water eventually overlies cool, fresher water. This situation is conducive to the formation of salt fingers (Turner 1979) and finger formation, as well as group of interleaving salt fingers are shown in figures 3(*g*) ($t =$ 98 min) and 3(*h*) ($t = 106$ mm), respectively. The finger behaviour is short-lived and no double-diffusive effects (species induced flow structure) were observed at $t_m =$ 111 min.

The qualitative behaviour of experiment D is representative of that observed in all of the tests. However, variations in the details of the flow were noted from experiment to experiment.

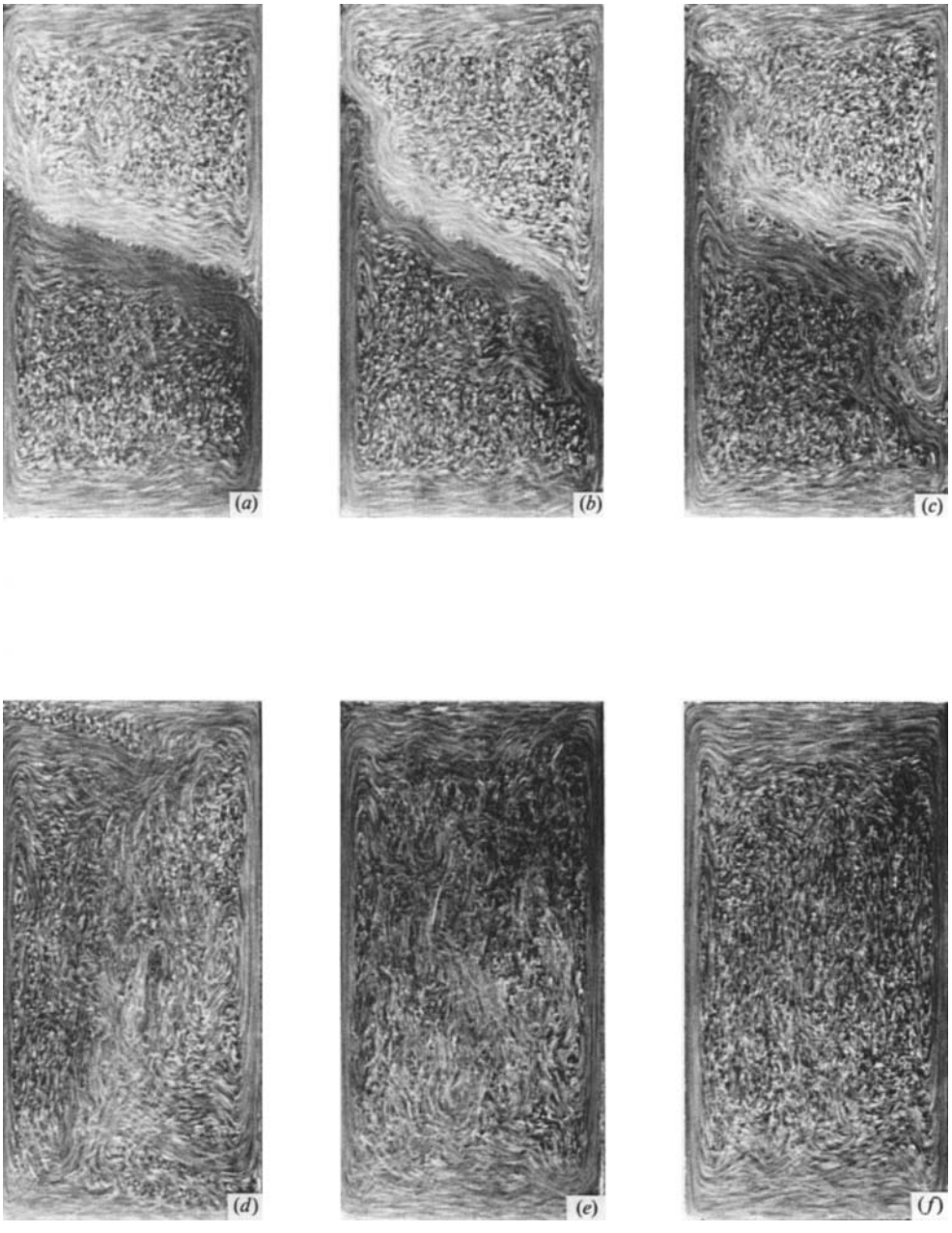

FIGURE 4. Flow visualization of experiment G. (*a*) $t = 20$ min; (*b*) $t = 30$ min; (*c*) $t = 40$ min; (*d*) $t = 45$ min; (*e*) $t = 48$ min; (*f*) $t = 53$ min.

Figure 4 shows flow visualization results for experiment G which is characterized by the same thermal and salinity conditions, but different aspect ratio, as experiment D. The general behaviour of this experiment again is characterized by a tilting interface (figure 4*a*, $t = 20$ min) which is subsequently penetrated by the sidewall boundary layers (figure 4*b*, $t = 30$ min; figure 4*c*, $t = 40$ min), interface rotation and

biased layer heating (figure 4*d*, $t = 45$ min) followed by finger formation (figure 4*e*, $t = 48$ min) and finally, mixed steady-flow (figure 4*f*, $t_m = 53$ min).

Several variations are noted between the results of figures 3 and 4. First, the interface tilt is more severe in experiment G than experiment D. This is expected since the temperature differences across the cell are the same and vertical boundary layers possess nearly equal momentum in both experiments. Hence, the overall interface deflections are approximately equal in both experiments rather than the interface tilt angle. Also of note is the absence of the flow reversal and the central vortex which were noted in the experiments with $A = 1$ (figures 3*e* and 3*f*, respectively).

Other variations in the detailed behaviour of the system were noted, the most important of which was interface migration. As the temperature difference across the test cell was increased, asymmetric behaviour was noted and can be attributed to variations in β_T with T. In these experiments (most noticeably in experiments E, F, K and M), the hot wall boundary layer penetrated the interface before the cold wall boundary layer. This non-Boussinesq behaviour resulted in a net transfer of fluid from the bottom layer to the top layer and, consequently, a falling interface. This effect has been noted in previous experiments (Wirtz & Reddy 1979). Although the presence of the migrating interface is undesirable from the standpoint of retaining system symmetry, it lends credibility to the hypothesized enhanced mixing due to the relatively high momentum vertical boundary layers which was discussed previously.

For the experiments associated with $R_{\rho,i} = 1.17$, the observed behaviour was nearly identical to that of the experiments with $R_{\rho,i} = 0.59$, except the interface tilt was initially less pronounced and the quasi-steady behaviour was extended. Of course, after the species concentration difference between the layers in experiments J–M decreases to the differences in the experiments with small $R_{\rho,i}$ system behaviour is identical.

3.2. *Mixing behaviour*

The results so far show that the detailed system behaviour is complicated. Coupled heat and species transfer are superimposed upon complex hydrodynamic phenomena at the salinity interface which is responsible for the system behaviour. The interface structure depends on the stabilizing influence of salt gradients and the destabilizing effects of temperature gradients and shear instabilities, as well as hydrodynamic forces associated with the vertical sidewall boundary layers and the test-cell aspect ratio. It is clear that a complete understanding of the detailed flow is impossible without correspondingly detailed salinity and velocity measurements. Unfortunately, such measurements would be very difficult due to the spatial variations of salinity which are expected to occur in both the layers (Wirtz 1977) as well as experimental difficulties involving electrical and optical techniques (Bergman, Incropera & Stevenson 1985).

Despite the complexity of the flow field, overall behaviour, in terms of relating t_m with appropriate parameters, can be described quite easily. Experimental results (t_m and $Fo_{c,m}$) are also shown in table 1 for each experiment. Since Pr and Sc are the same for all of the experiments, the dimensionless mixing time depends on Ra_T, $R_{\rho,i}$ and A.

The mixing relationship is shown in figure 5. For purposes of discussion, attention is first focused on the results for $R_{\rho,i} = 0.59$ and $A = 1.0$. For this set of experiments, the dimensionless mixing time decreases as Ra_T increases. This result is interesting, since, for a given $R_{\rho,i}$, ΔC_i is increased with ΔT. As such, even though more salt needs

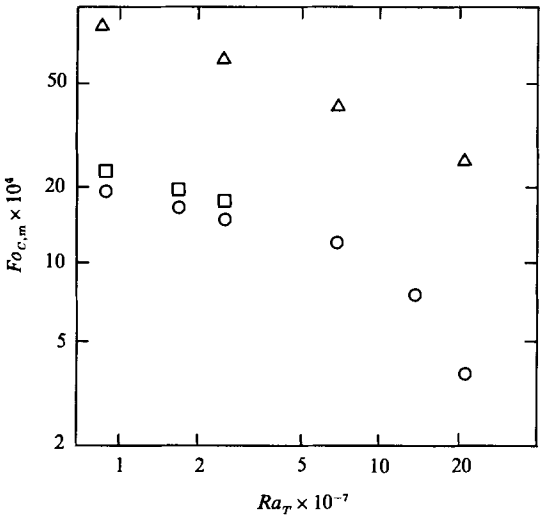

FIGURE 5. Dimensionless mixing time relationship. ○, $R_{\rho,i} = 0.59$, $A = 1.0$; □, $R_{\rho,i} = 0.59$, $A = 2.0$; $R_{\rho,i} = 1.17$, $A = 1.0$.

to be transferred through the interface as ΔT increases, convective velocities, and hence, species transfer rates across the salinity interface will increase with more vigorous heating and cooling and offset the increases in t_m associated with larger ΔC_i. The decrease in the dimensionless mixing time with Ra_T may also be attributed to the enhanced local salt transfer at the sidewalls of the enclosure, since more energetic vertical boundary layers exist with increasing Ra_T.

At the highest Ra_T and, to a lesser extent, at $Ra_T = 25.5 \times 10^6$ (experiment C), $Fo_{C,m}$ lies below a straight line which could be drawn through the other three data points. The decrease in $Fo_{C,m}$ for these experiments is attributed to the early penetration of the interface by the hot wall vertical boundary layers due to non-Boussinesq behaviour. In effect, the data points could be shifted to the right to reflect the effect of increased β_T at the hot wall.

As the initial density ratio is increased, ($R_{\rho,i} = 1.17, A = 1.0$), mixing times are substantially increased. This result is expected. Also of note, however, is the decreased curvature of the data which was, in the previous discussion, attributed to variation of β_T with T. Since the experiments with the larger $R_{\rho,i}$ are characterized by more stable interfaces, early penetration of the interface due to non-Boussinesq behaviour was not as influential on t_m as for the lower $R_{\rho,i}$ cases. Hence, the results for larger $R_{\rho,i}$ are not as susceptible to variations of β_T.

Finally, consideration is given to the influence of A on t_m. As evident, the dimensionless mixing time increases with the test-cell aspect ratio. Again, this result is expected and can be understood most readily by considering t_m as A approaches infinity. With an infinite amount of fluid to be mixed across a finite length interface spanning L, the mixing time will approach infinity as well.

3.3. *Interfacial species transport correlation*

The results of figure 5 may be used to correlate time-averaged salt transport rates across the salinity interface during quasi-steady behaviour.

Since all of the experiments were operated to t_m and since the thermal response of the system is relatively fast, the time required to transport enough salt across the

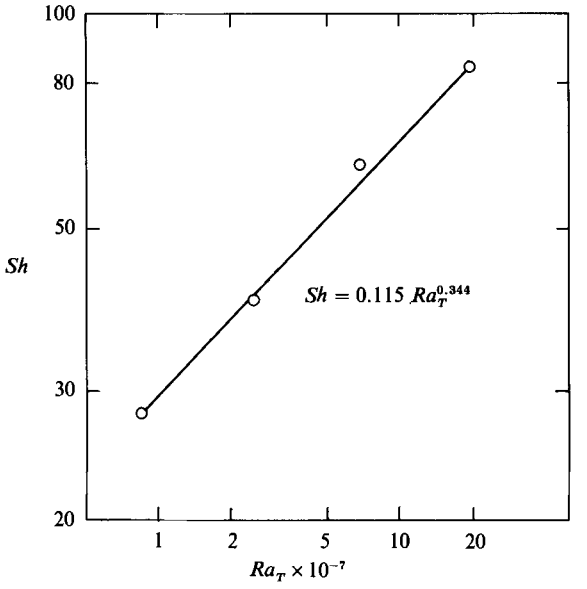

FIGURE 6. Interfacial salt transfer correlation.

interface so that ΔC_{i} for a high $R_{\rho,\mathrm{i}}$ experiment is reduced to the ΔC_{i} corresponding to a low $R_{\rho,\mathrm{i}}$ experiment is

$$t^* = t_{\mathrm{m,h}} - t_{\mathrm{m,l}}, \tag{11}$$

where $t_{\mathrm{m,h}}$ and $t_{\mathrm{m,l}}$ are the mixing times for the high and low $R_{\rho,\mathrm{i}}$ experiments, respectively. It should be noted that, in basing the following results on transport rates during t^*, mixing phenomena associated with vertical boundary layer penetration of the interface and finger behaviour are excluded from the interfacial species transport correlation.

The convective transport coefficient, h_{m}, describes the salt flux through the interface during quasi-steady behaviour

$$n_{\mathrm{s}} = h_{\mathrm{m}} \rho (C_2 - C_1). \tag{12}$$

As a first approximation, h_{m} is assumed to be constant during the quasi-steady period since the hydrodynamics of the system do not vary to a significant degree. By applying a species balance to the top fluid layer, h_{m} may be evaluated from

$$h_{\mathrm{m}} = \frac{-H}{4t^*} \ln\left(\frac{\Delta C_{\mathrm{i,l}}}{\Delta C_{\mathrm{i,h}}}\right). \tag{13}$$

The dimensionless salt transport coefficient (Sherwood number) may then be evaluated as

$$Sh = \frac{h_{\mathrm{m}} L}{D}. \tag{14}$$

The interfacial salt transport correlation for $A = 1$, $Pr = 6.5$ and $Sc = 550$ is shown in figure 6 and is described by

$$Sh = 0.115\, Ra_T^{0.344}, \tag{15}$$

with enhanced salt transport occurring with increasing Ra_T. Of course, a general correlation must include the influence of Pr and Sc.

4. Summary and conclusions

A two-layer, salt-stratified system destabilized by lateral heating and cooling has been investigated experimentally. Flow visualization reveals that the convective structure of the system is very complex. Diffusive and finger regime double-diffusion is evident early and late in the experiment, respectively. The interface separating the fluid layers is characterized by shear and thermal instabilities in competition with species stabilization. Vertical boundary layers on the heated and cooled sidewalls also influence system dynamics.

Despite the complexity of the details of the flow, the mixing time associated with layer merging is easily described with the relevant dimensionless parameters. Using information concerning the mixing time, the time-averaged interfacial salt transport during quasi-steady operation (Sh) is correlated with thermal buoyancy and viscous forces in the system (Ra_T).

The authors wish to acknowledge support of this work by The University of Texas at Austin University Research Institute and the National Science Foundation under Grant no. CBT-8552806.

REFERENCES

BERGMAN, T. L., INCROPERA, F. P. & STEVENSON, W. H. 1985 Miniature fiber optic refractometer for measurement of salinity in double-diffusive thermohaline systems. *Rev. Sci. Instrum.* **56**, 291–296.

HUPPERT, H. E., KERR, R. C. & HALLWORTH, M. A. 1984 Heating or cooling a stable compositional gradient from the side. *Intl J. Heat Mass Transfer* **27**, 1395–1401.

KAMOTANI, Y., WANG, L. W., OSTRACH, S. & JIANG, H. D. 1985 Experimental study of natural convection in shallow enclosures with horizontal temperature and concentration gradients. *Intl J. Heat Mass Transfer* **28**, 165–173.

LINDEN, P. F. & SHIRTCLIFFE, T. G. L. 1978 The diffusive interface in double-diffusive convection. *J. Fluid Mech.* **87**, 417–432.

MOORE, M. J. & LONG, R. R. 1971 An experimental investigation of turbulent stratified shearing flow. *J. Fluid Mech.* **49**, 635–655.

OSTRACH, S. 1980 Natural convection with combined driving forces. *PhysicoChemical Hydrodyn.* **1**, 233–247.

RHEE, H. S., KOSEFF, J. R. & STREET, R. L. 1984 Flow visualization of a recirculating flow by rheoscopic liquid and liquid crystal techniques. *Exp. Fluids* **2**, 57–64.

STICKLES, R. W., UNGAN, A. & VISKANTA, R. 1986 Natural convection in a rectangular enclosure with differentially heated end walls and a free liquid surface. *PhysicoChemical Hydrodyn.* **7**, 161–176.

TURNER, J. S. 1979 *Buoyancy Effects in Fluids.* Cambridge University Press.

WIRTZ, R. A. 1977 The effect of solute layering on lateral heat transfer in an enclosure. *Intl J. Heat Mass Transfer* **20**, 841–846.

WIRTZ, R. A. & REDDY, C. S. 1976 Heat and mass transport across diffusive interfaces bounded by turbulent connecting regions. *Intl J. Heat Mass Transfer* **19**, 471–478.

WIRTZ, R. A. & REDDY, C. S. 1979 Experiments on convective layer formation and merging in a differentially heated slot. *J. Fluid Mech.* **91**, 451–464.